Acta Cryst A FOUNDATIONS ADVANCES

ISSN 2053-2733

Structure of ordered coaxial and scroll nanotubes: general approach

Zufar Khalitov,* Azat Khadiev, Diana Valeeva and Dmitry Pashin

Nanotechnology in Electronics, Kazan National Research Technical University named after A. N. Tupolev, K. Marx 11, Kazan, Tatarstan 420111, Russian Federation. *Correspondence e-mail: zufar.khalitov@mail.ru

Received 17 August 2015
Accepted 14 October 2015

Edited by J.-G. Eon, Universidade Federal do Rio de Janeiro, Brazil

Keywords: multiwalled nanotubes; chiral nanotubes; scroll nanotubes; chiral indexes.

The explicit formulas for atomic coordinates of multiwalled coaxial and cylindrical scroll nanotubes with ordered structure are developed on the basis of a common oblique lattice. According to this approach, a nanotube is formed by transfer of its bulk analogue structure onto a cylindrical surface (with a circular or spiral cross section) and the chirality indexes of the tube are expressed in the number of unit cells. The monoclinic polytypic modifications of ordered coaxial and scroll nanotubes are also discussed and geometrical conditions of their formation are analysed. It is shown that tube radii of ordered multiwalled coaxial nanotubes are multiples of the layer thickness, and the initial turn radius of the orthogonal scroll nanotube is a multiple of the same parameter or its half.

1. Introduction

The development of multiwalled nanotube structural models has been carried out since the discovery of nanotubes in the 1950s. Long-term research has led to two approaches to the description of tube structure. According to the first approach, which was established by the pioneers of this field (Pauling, 1930; Warren *et al.*, 1931; Aruja, 1943; Bates *et al.*, 1950; Padurow, 1950; Whittaker, 1951, 1952, 1953; Noll & Kircher, 1951, 1952; Amelinckx *et al.*, 1996), a nanotube is formed by transferring the layer structure of the bulk analogue (carbon nanotube *versus* graphite, SnS_2 nanotube *versus* berndtite, SnS *versus* herzenbergite, WS_2 nanotube *versus* tungstenite) onto a cylindrical surface with a circular or spiral cross section (Fig. 1). The authors of the first approach have often used a rectangular non-primitive unit cell for the description of the nanotube structure. However, this approach has some limitations. The application of a non-primitive unit cell for constructing a seamless cylinder or a scroll could lead to the loss of some of the possible geometrical arrangements of atoms in a tube.

The second approach, which was developed after Iijima's (1991) discovery of carbon nanotubes, has been expanded only within structures with hexagonal symmetry (Hamada *et al.*, 1992; Saito *et al.*, 1998; Amelinckx *et al.*, 1999; Qin, 2006). However, it is hard to expect that all nanotubes will have hexagonal structure. For example, there are some reports about the synthesis of mixed-layer SnS/SnS_2 nanotubes with SnS layers having an orthorhombic structure (Hong *et al.*, 2003; Radovsky *et al.*, 2011). It is evident that in this case the chiral indexes, radius and chiral angle of a tube should be expressed in units of basis vectors of an orthorhombic, not a hexagonal, system. Consequently, these two approaches differ by the choice of the unit cell.

There is work (Bandura & Evarestov, 2009) that unites both presented approaches by implementing a universal oblique

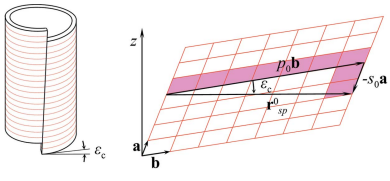

cell in the layer plane for single-walled nanotube formation. The authors also suggested that their procedure is appropriate both for single- and multiwalled nanotubes, even though, in the particular case of multiwalled carbon nanotubes, additional requirements for nanotube formation exist (Zhang *et al.*, 1993; Bernaerts *et al.*, 1998). Bandura & Evarestov (2009) did not discuss these peculiarities of multiwalled nanotube structure. In the common case of ordered multiwalled coaxial nanotubes with an arbitrary (but known) structure of the layer, as we will show in the present work, the list of additional requirements increases.

Despite the fact that there are a lot of articles associated with different aspects of scroll nanotube synthesis (Xie *et al.*, 2009; Cheng *et al.*, 2014; Zhao *et al.*, 2014) and structure (Jagodzinski & Kunze, 1954; Whittaker, 1955*b*; Yada, 1967, 1971; Yada & Iishi, 1977; DeVouard & Baronnet, 1995; Amelinckx *et al.*, 1996; Khalitov *et al.*, 2015), explicit formulas for coordinates of the atoms (similar to coaxial or bulk crystal cases) are absent. An exception to this is the work of the present authors, which was dedicated to the special case of nanotubes having rectangular unit cells and small chiral angles (Nasyrov *et al.*, 2010). There is also work (Enyashin & Seifert, 2005) associated with scroll nanotube formation where atomic coordinates of nanorolls are determined by a recursion procedure. However, the presented method has some disadvantages: for structural analysis it is more convenient to deal with atomic coordinates which are determined only by the number of the atom not by the coordinates of the previous atom.

The aim of this article is to develop a general approach for describing the structure of ordered multiwalled chiral coaxial and cylindrical scroll nanotubes, which will be based on a flat, oblique unit cell and chirality indexes expressed in the units of these cells. It is impossible to define a classic three-dimensional unit cell in cylindrical crystals because of uncertainty of the basis vector **c**. Therefore, a two-dimensional primitive unit cell (parallelogram) covers all structural cases and defines all possible geometrical arrangements of the atoms in the tube without loss. The definition 'ordered nanotube' means both regularity of the lattice on each layer and relative stacking of the layers. As opposed to conventional layered crystals, in nanotubes an interlayer ordering in a circumferential direction has a specific character. The unit cells of adjacent layers of a nanotube are unable to have equal relative positions in the circumferential direction because of the difference in curvature radius between these layers. Nevertheless, homological nodes of the adjacent layers are situated according to a certain law.

The planar layer of the bulk analogue can be considered as a development of the nanotube layer, which is oriented relative to the tube axis in a certain way (Fig. 2*a*). The existence of the tube axis, which can be treated as a reference direction, allows us to unambiguously define the positions of the main axes. Let us define the basis vectors of the lattice (see Appendix *A* for a list of the main parameters used in this paper) in such a way that the **b** vector has the direction that is closest to the cross-sectional plane of the tube. Consequently, the chiral angle ε_c can be defined as the angle between the **b** vector and this plane (Fig. 2*a*). The assumed positions of the main axes provide the interplanar spacings definition and diffraction spots notation that are similar to those of the bulk analogues of the nanotubes, from which the pioneering research in the field of cylindrical crystals began (Whittaker, 1954; Amelinckx *et al.*, 1996).

Let us define the two coordinate systems, which are tilted relative to each other by a chiral angle, in the nanotube's surface developed onto a plane: the system $\{a, b\}$ that is defined by the crystallographic basis and the rectangular $\{\xi, z\}$ system where the z axis is parallel to the axis of the tube (Figs. 1*a* and 2*a*). The position of the atom is defined by the vector $\mathbf{r}_{nvj} = \mathbf{r}_{nv} + \mathbf{r}_j$, where $\mathbf{r}_{nv} = n\mathbf{a} + v\mathbf{b}$ is the vector of the plane lattice, j is the unit number of the atom in the unit cell. The vector $\mathbf{r}_j$ defines the position of the atom in the projection of

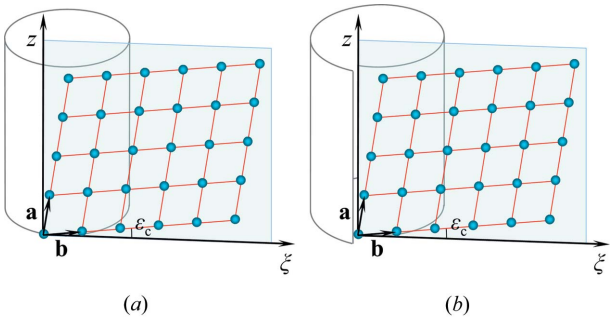

Figure 1
The transfer of the layer structure onto a cylindrical surface with (*a*) a circular and (*b*) a spiral cross section (the layer plane with coordinate systems $\{a, b\}$ and $\{\xi, z\}$, which is tangent to the surface at the point $\varphi = 0$, is indicated by the blue colour).

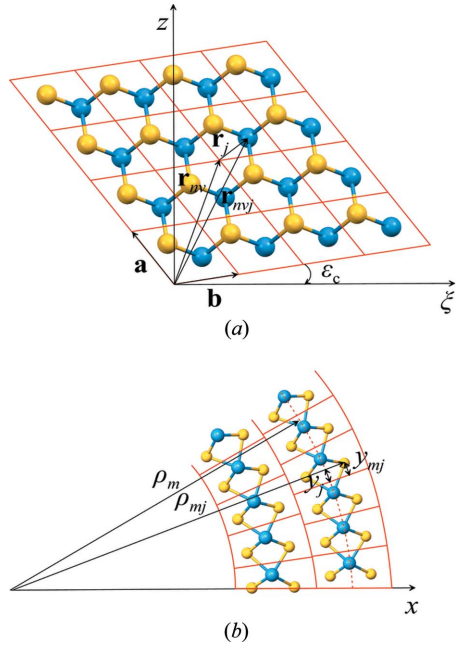

Figure 2
(*a*) The position of the planar layer relative to the tube axis z. (*b*) The determination of the circumferential coordinate of the atom.

the unit cell on a plane, and has x_j and y_j components in the **a** and **b** basis. These components are similar to the coordinates of the corresponding atoms in the unit cell of the bulk analogue. Consequently, the analytic formulas that perform the transformation of the initial $\{a, b\}$ coordinate system towards the new $\{\xi, z\}$ system depend on their relative positions (*i.e.* depend on the algebraic sign of the chiral angle ε_c). For example, the transformation $\{a, b\} \rightarrow \{\xi, z\}$ in Fig. 2(*a*) corresponds to a clockwise rotation and therefore the chiral angle ε_c is smaller than zero ($\varepsilon_c < 0$). It is more convenient to deal with the absolute value of the chiral angle, and for this reason we present the sign in the explicit form. Consequently, the atomic positions in the system $\{\xi, z\}$ are

$$\begin{cases} \xi_{nvj} = (an + x_j)\cos(\gamma \mp \varepsilon_c) + (bv + y_j)\cos\varepsilon_c \\ z_{nvj} = (an + x_j)\sin(\gamma \mp \varepsilon_c) \mp (bv + y_j)\sin\varepsilon_c, \end{cases} \quad (1)$$

where the lower sign corresponds to the clockwise transformation, and the upper sign to the anticlockwise transformation.

Contrary to coaxial nanotubes, in cylindrical scroll nanotubes the surface normal does not coincide with the radial direction in the cylindrical coordinate system. However, in the case of real nanotube radii this difference is so small that it might be neglected. One should choose an appropriate reference level for z_j coordinate determination. It is convenient to choose the origin of the unit cell on the reference radial level, where the circumferential length of the cell remains unaltered after bending of the layer (Whittaker, 1954; Baronnet *et al.*, 1994; DeVouard & Baronnet, 1995; Nasyrov *et al.*, 2010). This level, for example, corresponds to the level of the metal sheet in the chrysotile and WS_2 nanotubes; the x and y coordinates are determined on this reference level. Cylindrical bending produces expansion or compression of the circumferential coordinate of the atom on the other radial levels of the cell. Nevertheless, as can be seen later, this circumferential coordinate of the atom in the unit cell is presented in relation to its radial position in the cylindrical coordinate system. To illustrate this statement, let the y coordinate of the planar layer correspond to the circumferential direction. The reference level of the unit cell is presented in Fig. 2(*b*) by the dashed line, ρ_m is the radius of the corresponding mth layer, ρ_{mj} is the radius of the jth atom in the unit cell, y_{mj} is the circumferential coordinate of the jth atom in the unit cell and y_j is the corresponding atomic coordinate in the unit cell of the bulk analogue. According to this figure, it is evident that $y_{mj}/\rho_{mj} = y_j/\rho_m$. The obtained relation allows us to use the atomic coordinates of the bulk analogue for nanotube structure formation. The z axis coincides with the axis of the nanotube and, therefore, the second equation in (1) determines the z coordinates of the atoms. The transfer of the bulk analogue structure onto a cylindrical surface is performed by equating the length ξ_{nvj} to the circumference of a circle (for coaxial nanotubes) or to the length of a spiral turn (for cylindrical scroll nanotubes).

2. Structure of ordered multiwalled coaxial nanotubes

The relative positions of the layers in multiwalled coaxial nanotubes do not depend on each other. Therefore, interlayer shift determines all possible relative positions of the layers. Consequently, circumferential and longitudinal ordering are a polytypes issue and the clear examination of this question is not included in the aims of the presented work. In summary, only certain aspects of ordering in coaxial chiral nanotubes will be studied: namely, the radial packing of the layers, allowed chiral angles (chiral indexes) and regularity of the lattice on each layer.

The problem of radial packing arises from the requirements of close packing of adjacent layers in a multiwalled coaxial chiral nanotube and continuity of the lattice on each seamless tube. Whittaker first discussed the issue of close packing in a coaxial multiwalled nanotube with arbitrary parameters in the 1950s. He mentioned that the layers of a tube must have small imperfections (Whittaker, 1955*a*), and a perfect lattice is formed only when the relation $2\pi d/b$ (d is the layer thickness) is integer (Whittaker, 1954). Zhang *et al.* (1993) and Bernaerts *et al.* (1998) also treated the problem of close packing of the layers in tubes with hexagonal structure. They have achieved the conditions for close packing of the layers in a multiwalled coaxial carbon nanotube, but additional requirements for the tube radii were determined incompletely.

The results of the works presented above have shown that an ordered coaxial nanotube is formed only when special structural conditions are satisfied. In this paper, we will determine these conditions in terms of a selected general approach.

2.1. Ordered single-walled nanotube

Let ξ_{nvj} from equation (1) equate to the circumference of a circle with radius ρ_0:

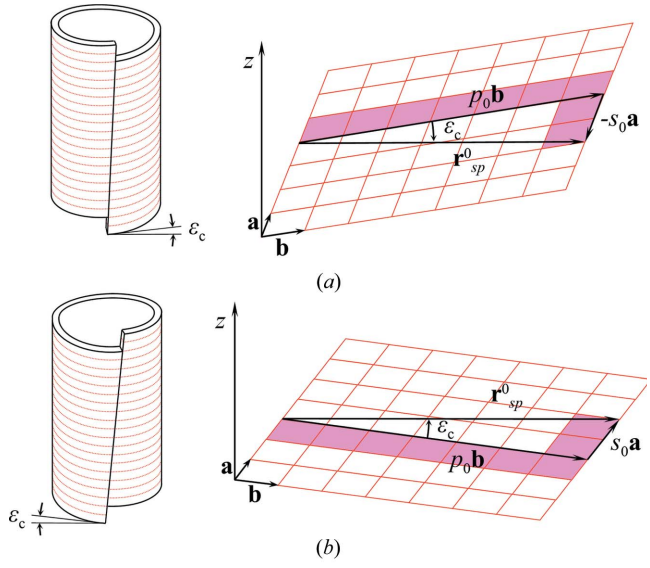

Figure 3
The definition of the chiral indexes for the right-handed (*a*) and left-handed (*b*) nanotubes.

$$\xi_{nvj} = \rho_0\varphi \rightarrow \varphi_{nvj} = \frac{1}{\rho_0}\left[(an + x_j)\cos(\gamma \mp \varepsilon_c) + (bv + y_j)\cos\varepsilon_c\right].$$

Consequently, the atomic coordinates of the ordered single-walled chiral nanotube in the cylindrical system $\{\rho, \varphi, z\}$ are

$$\begin{cases} \rho_{0j} = \rho_0 + z_j \\ \varphi_{nvj} = \frac{1}{\rho_0}\left[(an + x_j)\cos(\gamma \mp \varepsilon_c) + (bv + y_j)\cos\varepsilon_c\right] \\ z_{nvj} = (an + x_j)\sin(\gamma \mp \varepsilon_c) \mp (bv + y_j)\sin\varepsilon_c. \end{cases} \quad (2)$$

Fig. 3 represents the left- and right-handed single-walled chiral nanotubes and their developments. The handedness of the nanotube is determined by the nodal lines with n = const (v parameter increment direction). From Fig. 3 it is clearly seen that these lines form the right-handed helices if $\varepsilon_c < 0$ (Fig. 3*a*) and left-handed helices if $\varepsilon_c > 0$ (Fig. 3*b*). Consequently, from Fig. 2(*a*) and Fig. 3 it follows that the transformation $\{a, b\} \rightarrow \{\xi, z\}$ corresponds to clockwise rotation in right-handed tubes and to anticlockwise rotation in left-handed tubes. Therefore, the upper signs in equations (1) and (2) are attributed to the left-handed nanotube, and the lower signs to the right-handed nanotube. The presented definition of handedness is similar to the conventional one for carbon nanotubes (Bernaerts *et al.*, 1996), if a traditional primitive unit cell is chosen.

A seamless single-walled nanotube can be formed by rolling a single sheet around the z axis, which is perpendicular to any lattice vector (chiral vector) $\mathbf{r}^0_{sp} = \pm s_0\mathbf{a} + p_0\mathbf{b}$ (Fig. 3). According to this procedure, endpoints of the segment r^0_{sp} are superposed. The constructed single-walled chiral nanotube has the chiral indexes (s_0, p_0) that are defined in the unit-cell parameters. Such indexes have an apparent meaning: p_0 is the number of lattice nodes on the turn of the nodal line with n = const, and s_0 is the number of lattice nodes that determine the pitch of this line along the nodal row with v = const.

Trigonometric functions can be derived from the scalar products of corresponding vectors (Fig. 3):

$$\cos\varepsilon_c = \frac{p_0 b \pm s_0 a\cos\gamma}{2\pi\rho_0}, \quad \cos(\gamma \mp \varepsilon_c) = \frac{p_0 b\cos\gamma \pm s_0 a}{2\pi\rho_0},$$
$$\sin\varepsilon_c = \frac{s_0 a\sin\gamma}{2\pi\rho_0}, \quad \sin(\gamma \mp \varepsilon_c) = \frac{p_0 b\sin\gamma}{2\pi\rho_0},$$
$$2\pi\rho_0 = r^0_{sp} = \left[(s_0 a)^2 \pm 2s_0 p_0 ab\cos\gamma + (p_0 b)^2\right]^{1/2}. \quad (3)$$

By plugging equation (3) into equation (2) we get the atomic coordinates of the ordered single-walled chiral nanotube with the chiral indexes (s_0, p_0):

$$\begin{cases} \rho_{0j} = \rho_0 + z_j \\ \varphi_{nvj} = \frac{1}{2\pi\rho_0^2}\left[(an + x_j)(p_0 b\cos\gamma \pm s_0 a) + (bv + y_j)(p_0 b \pm s_0 a\cos\gamma)\right] \\ z_{nvj} = \frac{\sin\gamma}{2\pi\rho_0}\left[(an + x_j)p_0 b \mp (bv + y_j)s_0 a\right]. \end{cases} \quad (4)$$

2.2. Ordered multiwalled coaxial nanotube

A close-packed ordered multiwalled nanotube can be treated as a set of coaxial cylinders with radii being terms of arithmetic progression:

$$\rho_m = \rho_0 + md, \quad (5)$$

where ρ_0 is the inner radius of a tube, d the layer thickness and m the unit number of the layer that begins from zero. In the same way as in the previous section, one can define the magnitude of the chiral vector for each cylinder and the corresponding trigonometric functions:

$$r^m_{sp} = 2\pi\rho_m = \left[(s_m a)^2 \pm 2s_m p_m ab\cos\gamma + (p_m b)^2\right]^{1/2},$$
$$\cos\varepsilon_{cm} = \frac{p_m b \pm s_m a\cos\gamma}{2\pi\rho_m},$$
$$\cos(\gamma \mp \varepsilon_{cm}) = \frac{p_m b\cos\gamma \pm s_m a}{2\pi\rho_m}$$
$$\sin\varepsilon_{cm} = \frac{s_m a\sin\gamma}{2\pi\rho_m}, \quad \sin(\gamma \mp \varepsilon_{cm}) = \frac{p_m b\sin\gamma}{2\pi\rho_m}, \quad (6)$$

where s_m and p_m are the chiral indexes of the mth layer (s_m, p_m). The formulas (4)–(6) allow us to deduce the atomic coordinates of the multiwalled coaxial nanotube:

$$\begin{cases} \rho_{mj} = \rho_m + z_j \\ \varphi_{mnvj} = \frac{1}{2\pi\rho_m^2}\left[(an + x_j)(p_m b\cos\gamma \pm s_m a) + (bv + y_j)(p_m b \pm s_m a\cos\gamma)\right] + \varepsilon_m \\ z_{mnvj} = \frac{\sin\gamma}{2\pi\rho_m}\left[(an + x_j)p_m b \mp (bv + y_j)s_m a\right] + \Delta z_m, \end{cases} \quad (7)$$

where ε_m and Δz_m are the circumferential and longitudinal shift of the mth layer relative to the common reference point, respectively.

Fig. 4(*a*) shows the three-dimensional representations of the orthogonal nanotube (ε_m = 0, Δz_m = 0) development, consisting of several layers. Fig. 4(*b*) reveals the border regions of layer developments with the m (red lines) and

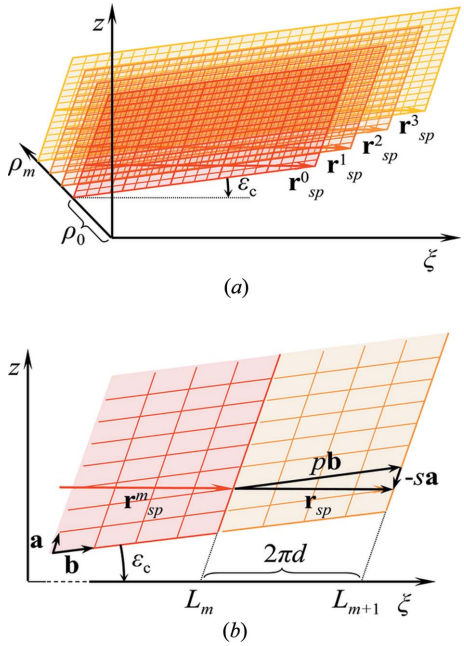

Figure 4
(*a*) The developments of the orthogonal chiral nanotube layers. (*b*) The border regions of the adjacent layers developed onto a plane.

$(m + 1)$ (yellow lines) index numbers of the same tube. The chiral vectors $\mathbf{r}_{sp}^{m}$, that are also shown in Figs. 4(*a*) and 4(*b*), are parallel to each other, because all of them are perpendicular to the same tube axis. From equation (5) it follows that the circumference of the circle L_m and therefore the magnitude of the corresponding chiral vector increase by the same value $2\pi d$ when passing from one layer to another:

$$L_m = 2\pi\rho_m = 2\pi\rho_0 + 2\pi dm \rightarrow L_{m+1} - L_m = 2\pi d.$$

The value $2\pi d$ is the length of the so-called 'unit' circle with the radius d. Consequently, the magnitudes of the chiral vectors can be expressed as

$$r_{sp}^{m} = L_m = 2\pi\rho_0 + 2\pi dm = r_{sp}^{0} + mr_{sp}, \quad r_{sp}^{0} = 2\pi\rho_0,$$
$$r_{sp} = 2\pi d. \tag{8}$$

Chiral vectors are parallel to each other and, therefore, the simple vector equality can be written as

$$\mathbf{r}_{sp}^{m} = \mathbf{r}_{sp}^{0} + m\mathbf{r}_{sp}, \tag{9}$$

where $\mathbf{r}_{sp}$ is the vector with the magnitude given in (8). This vector is parallel to the chiral vector.

From equation (9) it follows that the vector $\mathbf{r}_{sp} = \pm s\mathbf{a} + p\mathbf{b}$ is also the lattice vector with the magnitude

$$r_{sp} = [(sa)^2 \pm 2spab\cos\gamma + (pb)^2]^{1/2} = 2\pi d. \tag{10}$$

It turns out that the existence of the lattice vector with magnitude equal to the length of the 'unit' circle is necessary for seamless multiwalled coaxial nanotube formation. If an appropriate value of γ is chosen, expression (10) transforms to another condition achieved for close-packed multiwalled carbon nanotubes (Bernaerts *et al.*, 1998).

The chiral vectors' parallelism also leads to the vector equality

$$\mathbf{r}_{sp}^{m} = \lambda_m \mathbf{r}_{sp}^{0},$$

where λ_m parameters can be found from equation (8):

$$\lambda_m = 1 + \frac{d}{\rho_0}m \quad \rightarrow \quad \mathbf{r}_{sp}^{m} = \mathbf{r}_{sp}^{0} + \frac{d}{\rho_0}\mathbf{r}_{sp}^{0}m. \tag{11}$$

By comparing equations (9) and (11), one can achieve

$$\mathbf{r}_{sp} = \frac{d}{\rho_0}\mathbf{r}_{sp}^{0} \quad \rightarrow \quad \pm s\mathbf{a} + p\mathbf{b} = \pm\frac{d}{\rho_0}s_0\mathbf{a} + \frac{d}{\rho_0}p_0\mathbf{b}, \tag{12}$$

or, after expanding equation (12) in components,

$$\begin{cases} s_0 = s\frac{\rho_0}{d} \\ p_0 = p\frac{\rho_0}{d} \end{cases} \quad \rightarrow \quad \rho_0 = m_0 d, \tag{13}$$

where m_0 is an integer in general. The achieved result [equation (13)] means that the ordered coaxial chiral lattice should be multiple. In other words, the inner radius of the tube should be a multiple of the layer thickness. It is a sufficient condition for the ordered multiwalled coaxial nanotube formation. Consequently, we have

$$s_0 = sm_0, \quad p_0 = pm_0, \quad s_m = s(m_0 + m), \quad p_m = p(m_0 + m). \tag{14}$$

From equations (5), (6), (13) and (14) it follows that

$$\sin\varepsilon_{cm} = \frac{sa\sin\gamma}{2\pi d} = \sin\varepsilon_c,$$
$$\sin(\gamma \mp \varepsilon_{cm}) = \frac{pb\sin\gamma}{2\pi d} = \sin(\gamma \mp \varepsilon_c),$$
$$\cos\varepsilon_{cm} = \frac{pb \pm sa\cos\gamma}{2\pi d} = \cos\varepsilon_c,$$
$$\cos(\gamma \mp \varepsilon_{cm}) = \frac{pb\cos\gamma \pm sa}{2\pi d} = \cos(\gamma \mp \varepsilon_c). \tag{15}$$

The presented expressions show that the ordered coaxial nanotube should be monochiral. The achieved expressions allow us to use (2) for defining the atomic coordinates of the ordered multiwalled coaxial nanotube:

$$\begin{cases} \rho_{mj} = \rho_m + z_j \\ \varphi_{mnvj} = \frac{1}{\rho_m}\left[(an + x_j)\cos(\gamma \mp \varepsilon_c) + (bv + y_j)\cos\varepsilon_c\right] + \varepsilon_m \\ z_{mnvj} = (an + x_j)\sin(\gamma \mp \varepsilon_c) \mp (bv + y_j)\sin\varepsilon_c + \Delta z_m. \end{cases}$$

As was mentioned, the ordered coaxial nanotube could be formed only if a, b and d parameters of the bulk analogue satisfy equation (10). Put another way, the magnitude of a certain lattice vector must be equal to the length of the 'unit' circle. Let us call this vector or the pair of its components (s, p) a generator of a cylindrical lattice. From equation (15) it follows that the components of the generator are

$$s = \frac{2\pi d}{a\sin\gamma}\sin\varepsilon_c, \quad p = \frac{2\pi d}{b\sin\gamma}\sin(\gamma \mp \varepsilon_c). \tag{16}$$

The components being structural constants (because they are expressed in terms of the structural constants) characterize the ability of the planar layer to form a regular cylindrical lattice. It is easy to show that the chiral vectors of the multiple coaxial cylindrical lattice are divisible by the generator of this lattice: $\mathbf{r}_{sp}^{m} = \pm(s_0 + sm)\mathbf{a} + (p_0 + pm)\mathbf{b} = \pm(m_0 + m)s\mathbf{a} + (m_0 + m)p\mathbf{b} = (m_0 + m)\mathbf{r}_{sp}$.

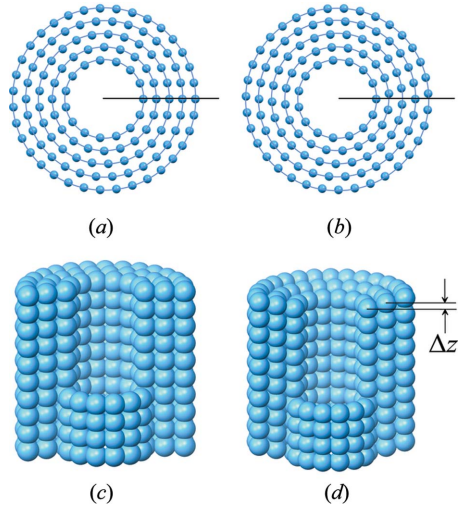

Figure 5
Multiple achiral coaxial lattices. (*a*) Orthogonal ($m_0 = 3$), top view. (*b*) Azimuthally monoclinic ($m_0 = 3$, $\Delta b = b/3$), top view. (*c*) Orthogonal ($m_0 = 2$), side view. (*d*) Longitudinally monoclinic ($m_0 = 2$, $\Delta a = a/3$), side view.

As was mentioned earlier (Whittaker, 1954), the formation of an achiral coaxial chrysotile nanotube requires an integer value of $p = 2\pi d/b$, which is the particular case with $s = 0$. Consequently, $\mathbf{r}_p = p\mathbf{b}$ is the generator of an achiral coaxial lattice with integer p.

The generator (or its components) is a combination of structural constants of the nanotube layers, which unambiguously define their chiral angles. Consequently, each variety of an ordered monochiral nanotube being monochiral has its own 'special' chiral angle. For example, the issue of the 'special' chiral angles in coaxial close-packed carbon nanotubes was studied in Bernaerts *et al.* (1998). After taking into account possible deviations of the tube's structure from the ordered coaxial or orthogonal scroll structures, it was possible to consider that chiral angles of a certain variety of the tube will group near a 'special' value.

Circumferential and longitudinal shifts, which are accordingly characterized by linear (Δz_m) and angular ($\varepsilon_m = \Delta\xi_m/\rho_m$) parameters, determine the polytypes of coaxial nanotubes. The most prominent ones are monoclinic polytypes with $\varepsilon_m = m\Delta\xi/\rho_m$ (Fig. 5*b*) and $\Delta z_m = m\Delta z$ (Fig. 5*d*). Δz and $\Delta\xi$ could be written in terms of Δa and Δb, which define a shift of one layer relative to another along the corresponding basis vectors (Figs. 5*b* and 5*d*):

$$\Delta\xi = \Delta a\cos(\gamma \mp \varepsilon_c) + \Delta b\cos\varepsilon_c,$$
$$\Delta z = \Delta a\sin(\gamma \mp \varepsilon_c) \mp \Delta b\sin\varepsilon_c.$$

It is evident that the interlayer shifts are determined only within a magnitude of the lattice basis vector.

3. Structure of scroll nanotubes

The presented method for describing the structure of scroll nanotubes is based on the Archimedean spiral. It is known that the distance between successive turns of the Archimedean spiral, in contrast to the involute of the circle having a constant separation distance, depends on the radius. However, this dependence plays a significant role only when the inner radius is very small. The above-mentioned peculiarity and simplicity of the Archimedean spiral's analytic expression allow us to choose this type of spiral for describing scroll structures.

Cylindrical scroll nanotubes are close packed and monochiral by definition. Therefore, the problems of radial packing and allowed chiral angles of the layers in the scroll tubes, in contrast to the coaxial case, do not arise. Consequently, the term 'ordered scroll nanotube' rather means the character of the interlayer shift in a multiwalled scroll lattice, which is also treated here using developments of the layers. The interlayer shift depends on the inner radius of the tube ρ_0 and chiral angle ε_c. A change of ε_c leads to rotation of the layers and mainly to the relative shift of the turns in the longitudinal direction of the tube, whereas ρ_0 deviations produce the relative shift of the turns in the circumferential (azimuthal) direction. Therefore, nanotubes with these relative shifts of the layers form the polytypic modifications of the scroll tubes, namely the longitudinal and azimuthal modifications. Monoclinic polytypic modifications are treated as deviations from orthogonal structure in which each full turn contains the integer number of the unit cells.

3.1. Flat spiral

The formula that describes the Archimedean spiral with the inner radius ρ_0 and pitch d has the form

$$\rho = \rho_0 + \tau\Phi, \quad \tau = \frac{d}{2\pi}, \tag{17}$$

where ρ and Φ are polar coordinates. The handedness of the flat spiral is determined by the algebraic sign of the τ parameter ($\tau > 0$ for the right-handed spiral, $\tau < 0$ for the left-handed spiral). Let us express the length of the spiral $\xi(\Phi)$ [equation (17)] in terms of a polar angle:

$$\begin{aligned}
\mathrm{d}\rho &= \tau\mathrm{d}\Phi,\\
\mathrm{d}\xi &= (\mathrm{d}\rho^2 + \rho^2\mathrm{d}\Phi^2)^{1/2} = [\tau^2 + (\rho_0 + \tau\Phi)^2]^{1/2}\mathrm{d}\Phi,\\
\xi(\Phi) &= \int_0^{\Phi}[\tau^2 + (\rho_0 + \tau\Phi)^2]^{1/2}\mathrm{d}\Phi\\
&= \frac{\rho_0 + \tau\Phi}{2\tau}[\tau^2 + (\rho_0 + \tau\Phi)^2]^{1/2} - \frac{\rho_0}{2\tau}(\tau^2 + \rho_0^2)^{1/2}\\
&\quad + \frac{\tau}{2}\ln\frac{\rho_0 + \tau\Phi + [\tau^2 + (\rho_0 + \tau\Phi)^2]^{1/2}}{\rho_0 + (\tau^2 + \rho_0^2)^{1/2}}.
\end{aligned} \tag{18}$$

Usually, in real tubes ρ_0 and Φ are relatively large values. This factor allows us to neglect the logarithmic member and the τ^2 term under the radical. The proposed approximation and relation (17) lead to the basic relations that govern the further development of the explicit formulas for describing scroll nanotube structure:

$$\begin{cases} \xi(\Phi) = \rho_0\Phi + \frac{\tau\Phi^2}{2} \\ \xi(\rho) = \frac{\rho^2 - \rho_0^2}{2\tau}, \end{cases} \quad \begin{cases} \Phi(\xi) = \frac{1}{\tau}(\rho_0^2 + 2\tau\xi)^{1/2} - \frac{\rho_0}{\tau} \\ \rho(\xi) = (\rho_0^2 + 2\tau\xi)^{1/2}. \end{cases} \tag{19}$$

This approximation is relatively good, except for the case when ρ_0 is small. The neglected logarithmic term is only a small (hundredths of one per cent) fraction of the algebraic one. It seems that small values of ρ_0 will lead to increasing flexure and thus strains in the layer. Therefore the existence of a small inner radius has low probability and the proposed approximation will cover the most practical cases.

Let us divide the spiral [equation (17)] into the turns. The length ξ_m along the spiral to the beginning of the mth turn could be deduced from equation (19):

$$\Phi_m = 2\pi m \rightarrow \xi_m = 2\pi\rho_0 m + \pi m^2 d. \tag{20}$$

The radius of the turn at its initial (reference) point is

$$\rho_m = \rho_0 + \tau\Phi_m = \rho_0 + md,$$

which is similar to equation (5). It is easy to introduce an azimuthal variable φ that begins from zero at each turn by using expression (19):

$$\rho(\varphi) = \rho_0 + \tau(\Phi_m + \varphi) = \rho_0 + md + \tau\varphi = \rho_m + \tau\varphi$$
$$\rightarrow \varphi = \frac{1}{\tau}(\rho - \rho_m). \quad (21)$$

The length of the spiral's mth turn is

$$L_m = \xi_{m+1} - \xi_m = 2\pi\rho_0 + 2\pi md + \pi d = 2\pi\rho_m + \pi d, \quad (22)$$

and the difference between the two adjacent turns

$$\Delta L_m = L_{m+1} - L_m = 2\pi d. \quad (23)$$

It is clearly seen that, when passing from one layer to another, the length of the turn changes by the same amount as in a coaxial tube. Comprehensive mathematical analysis shows that, after taking into account the logarithmic term in equation (18), the difference [equation (23)] does not become a constant, but it tends to $2\pi d$ if ρ_0 is relatively large. This result, which was also achieved in DeVouard & Baronnet (1995), essentially simplifies derivations of the structural formulas and allows us to perform comparative studies of coaxial and scroll structures.

The length of the spiral's arc as a function of an angle φ can be deduced from equations (19) and (20):

$$\xi(\Phi_m + \varphi) - \xi_m = \frac{\tau(2\pi m + \varphi)^2}{2} - \pi d m^2 = \rho_m\varphi + \frac{\tau\varphi^2}{2}. \quad (24)$$

3.2. Single-walled cylindrical scroll nanotube

The formation of a single-walled cylindrical scroll nanotube could be treated in a similar way to the coaxial nanotube. Fig. 6(a) represents the scroll nanotube turn. The plane unrolled lattice of this turn, which can be described by the vector $\mathbf{r}_{nv} = n\mathbf{a} + v\mathbf{b}$, is represented in Fig. 6(b). From Figs. 6(a) and 6(b) it is seen that by rolling of the layer around the z axis, which is perpendicular to any lattice vector $\mathbf{r}^0_{sp} = \pm s_0\mathbf{a} + p_0\mathbf{b}$, the scroll orthogonal nanotube could be formed. According to this procedure the ends of the segment r^0_{sp} lie on the same radial line in the cylindrical system $\{\rho, \varphi, z\}$, and the distance between these two points is equal to d. Meanwhile, the segment r^0_{sp} transforms into the spiral with length governed by formula (22) at m = 0:

$$r^0_{sp} = [(s_0a)^2 \pm 2s_0p_0ab\cos\gamma + (p_0b)^2]^{1/2} = L_0 = 2\pi\rho_0 + \pi d.$$

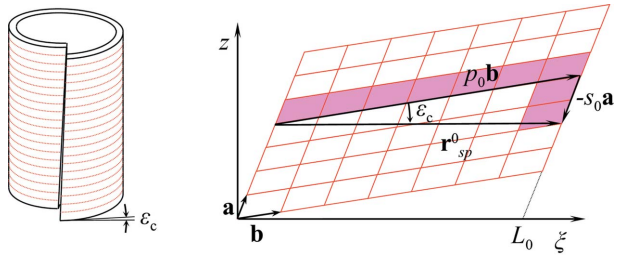

(a) (b)

Figure 6
(a) Single-walled right-handed scroll nanotube and (b) the development of its lattice.

Consequently, in the case of the scroll structure we can also use the concepts of the chiral vector $\mathbf{r}^0_{sp}$ and chiral indexes (s_0, p_0). The upper signs in the presented expressions are attributed to the left-handed scroll nanotube, and the lower signs to the right-handed nanotube.

Let us deduce the atomic coordinates of the single-walled scroll nanotube by transfer of the planar layer onto a scroll turn with inner radius ρ_0. As was mentioned, it can be done by equating ξ_{nvj} from equation (1) to the length of the flat spiral turn [equation (24)] at m = 0:

$$\rho_0\varphi + \frac{\tau\varphi^2}{2} = \xi_{nvj} \rightarrow \varphi_{nvj} = \frac{1}{\tau}\Big(\big\{\rho_0^2 + 2\tau[(an + x_j)\cos(\gamma \mp \varepsilon_c) + (bv + y_j)\cos\varepsilon_c]\big\}^{1/2} - \rho_0\Big).$$

We plug the achieved expression into equation (17), perform a change of the variable $\Phi \rightarrow \varphi$ and add the radial coordinate of the atom z_j; as a result, we get

$$\rho_{nvj} = \rho_0 + \tau\varphi_{nvj} + z_j = \big\{\rho_0^2 + 2\tau[(an + x_j)\cos(\gamma \mp \varepsilon_c) + (bv + y_j)\cos\varepsilon_c]\big\}^{1/2} + z_j.$$

Consequently, the atomic coordinates are

$$\begin{cases} \rho_{nvj} = \big\{\rho_0^2 + 2\tau[(an + x_j)\cos(\gamma \mp \varepsilon_c) \\ \qquad +(bv + y_j)\cos\varepsilon_c]\big\}^{1/2} + z_j \\ \varphi_{nvj} = \frac{1}{\tau}\big(\{\rho_0{}^2 + 2\tau[(an + x_j)\cos(\gamma \mp \varepsilon_c) \\ \qquad +(bv + y_j)\cos\varepsilon_c]\big\}^{1/2} - \rho_0\big) \\ z_{nvj} = (an + x_j)\sin(\gamma \mp \varepsilon_c) \mp (bv + y_j)\sin\varepsilon_c, \end{cases} \quad (25)$$

where the trigonometric functions can be expressed in terms of the chiral indexes using equation (3). After that, expression (25) will transform into

$$\begin{cases} \rho_{nvj} = \big\{\rho_0^2 + \frac{2\tau}{r^0_{sp}}[(an + x_j)(p_0b\cos\gamma \pm s_0a) \\ \qquad +(bv + y_j)(p_0b \pm s_0a\cos\gamma)]\big\}^{1/2} + z_j \\ \varphi_{nvj} = \frac{1}{\tau}\big(\{\rho_0{}^2 + \frac{2\tau}{r^0_{sp}}[(an + x_j)(p_0b\cos\gamma \pm s_0a) \\ \qquad +(bv + y_j)(p_0b \pm s_0a\cos\gamma)]\big\}^{1/2} - \rho_0\big) \\ z_{nvj} = \frac{\sin\gamma}{r^0_{sp}}[(an + x_j)p_0b \mp (bv + y_j)s_0a]. \end{cases}$$

3.3. Orthogonal multiwalled cylindrical scroll nanotube

The development of the multiwalled scroll nanotube with the border regions of its turns and corresponding chiral

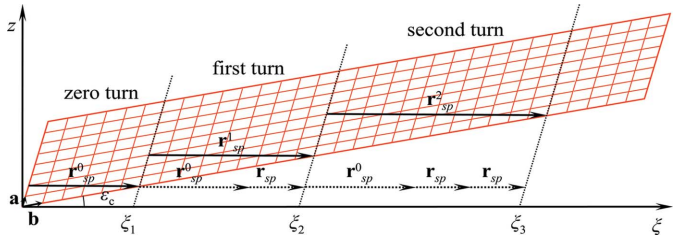

Figure 7
The development of the right-handed orthogonal scroll nanotube.

vectors $\mathbf{r}_{sp}^{m}$ is represented in Fig. 7. It is evident that the borders of the turns can be chosen arbitrarily to some extent. But we suppose that it is more convenient to hold the lines that go parallel to **a** through ξ_m points as the borders of the turn.

Let us study the chiral vectors of a multiwalled scroll nanotube belonging to an orthogonal polytypic modification. According to the definition, the dimensions of the turns are determined by the integer numbers of the unit cells p_m and s_m. These parameters are counted in the directions parallel to the lattice basis vectors. According to equations (22) and (23) the magnitude of the chiral vector that corresponds to the mth turn can be expressed as

$$r_{sp}^{m} = L_m = r_{sp}^{0} + mr_{sp} = 2\pi\rho_0 + \pi d + 2\pi dm,$$
$$r_{sp}^{0} = 2\pi\rho_0 + \pi d, \quad r_{sp} = 2\pi d. \tag{26}$$

Chiral vectors of the different turns are parallel to each other and, therefore, one can write the vector equality:

$$\mathbf{r}_{sp}^{m} = \pm s_m\mathbf{a} + p_m\mathbf{b} = \mathbf{r}_{sp}^{0} + m\mathbf{r}_{sp}, \quad \mathbf{r}_{sp}^{0} = \pm s_0\mathbf{a} + p_0\mathbf{b}, \tag{27}$$

where $\mathbf{r}_{sp}$ is the vector with the magnitude

$$r_{sp} = [(sa)^2 \pm 2spab\cos\gamma + (pb)^2]^{1/2} = 2\pi d.$$

The vector $\mathbf{r}_{sp}$ is also parallel to the chiral vectors. From equation (27) it also follows that vectors $\mathbf{r}_{sp}^{m}$, $\mathbf{r}_{sp}^{0}$ and $\mathbf{r}_{sp} = \pm s\mathbf{a} + p\mathbf{b}$ are the lattice vectors of the planar layer, and the chiral indexes in the scroll nanotube are similar to the coaxial ones:

$$s_m = s_0 + sm, \quad p_m = p_0 + pm,$$

with integer s and p. In this case we also get a generator [equation (10)] with integer components [equation (16)] as in coaxial tubes. The achieved result shows that it is necessary to have integer components of the generator for orthogonal scroll lattice formation.

As in coaxial tubes, the parallelism of the chiral vectors in the scroll structures leads to the expression

$$s_0 = s\left(\frac{\rho_0}{d} + \frac{1}{2}\right), \quad p_0 = p\left(\frac{\rho_0}{d} + \frac{1}{2}\right). \tag{28}$$

The integral property of s_0 and p_0 for any s and p holds only if

$$\frac{\rho_0}{d} + \frac{1}{2} = m_0 \rightarrow \rho_0 = \left(m_0 - \frac{1}{2}\right)d, \tag{29}$$

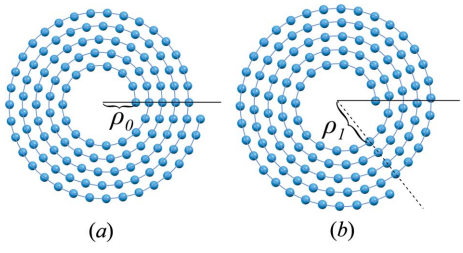

Figure 8
Examples of equivalent orthogonal scroll lattices. (*a*) Scroll lattice with the multiple inner radius. (*b*) Similar lattice in which the first two nodes are removed.

where m_0 is an integer. Consequently, the integral property is fulfilled in the case of a semi-multiple lattice, in which the inner radius is equal to the half-integer value of the d parameter. In the particular case of even s and p, the integral property of s_0 and p_0 holds (similar to coaxial tubes) if the cylindrical lattice is multiple [equation (13)].

The chiral indexes for both cases can be expressed as

$$s_m = s(m_0 + m), \quad p_m = p(m_0 + m),$$

and the magnitude of the chiral vector is

$$r_{sp}^{m} = 2\pi\rho_0 + \pi d + 2\pi dm = (m_0 + m)r_{sp}. \tag{30}$$

In cylindrical scroll tubes, chiral vectors are also divisible by a generator of this lattice. The sufficient condition for orthogonal scroll lattice formation for any s and p is the semi-multiple inner radius, while for the particular case of even s and p, it is the multiple inner radius.

It should be noticed that orthogonal scroll lattices have a radial direction in which lattice nodes of the adjacent layers lie along a straight line. When constructing the structure of an orthogonal scroll nanotube, such a direction is usually defined by the first node. In some cases such a direction might be defined by another (not a first) node. This peculiarity addresses the issue of the equivalent scroll lattices. Figs. 8(*a*) and 8(*b*) represent examples of the plane orthogonal scroll lattices with $p = 5$ and $m_0 = 3$. The coordinates of the nodes of such lattices can be deduced from equation (25) at $n = \varepsilon_c = x_j = y_j = z_j = 0$, $\gamma = 90^\circ$, $\rho_0 \rightarrow \rho_m$. At first glance, the lattice (*a*) appears to differ from (*b*). However, the second lattice is achieved from the first one by vanishing of the two initial nodes (the reference position of the line, on which the nodes of the adjacent layers lie, is marked by the dashed line). Consequently, two scroll lattices are equivalent if they can be treated as part of a certain scroll lattice. This allows us to apply the results achieved for the orthogonal scroll lattice to any equivalent lattice after appropriate transformation of the node indexes.

Transfer of the bulk analogue structure onto the scroll lattice requires coordinates of the initial nodes ($n = 0$, $v = 0$) on each turn. Fig. 9 reveals the border regions of the turns' developments with the m and (m + 1) index numbers of the

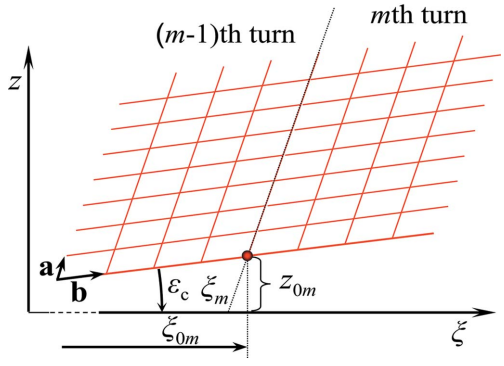

Figure 9
The determination of the initial node coordinates of the turn that corresponds to the right-handed scroll nanotube.

same tube. The initial node of the mth turn is represented by the red point. From Fig. 9 and expression (19) it follows that

$$z_{0m} = \mp P_m b \sin\varepsilon_c,\ \xi_{0m} = P_m b \cos\varepsilon_c \rightarrow \rho_{0m} = (\rho_0^2 + 2\tau\xi_{0m})^{1/2},$$

where

$$P_m = \sum_{m'=0}^{m-1} p_{m'} = p\left(m_0 + \frac{m-1}{2}\right)m. \tag{31}$$

Thus, the cylindrical atomic coordinates of the orthogonal scroll nanotube can be achieved from equation (25). The φ and ρ coordinates require usage of equation (21) and changing of the variable $\rho_0 \rightarrow \rho_{0m}$, while the z coordinate requires only addition of z_{0m} to its initial value. After that, one can achieve

$$\begin{cases} \rho_{mnvj} = \{\rho_{0m}^2 + 2\tau[(an + x_j)\cos(\gamma \mp \varepsilon_c) \\ \qquad +(bv + y_j)\cos\varepsilon_c]\}^{1/2} + z_j \\ \varphi_{mnvj} = \frac{1}{\tau}\left(\{\rho_{0m}^2 + 2\tau[(an + x_j)\cos(\gamma \mp \varepsilon_c) \right. \\ \qquad \left. +(bv + y_j)\cos\varepsilon_c]\}^{1/2} - \rho_m\right) \\ z_{mnvj} = z_{0m} + (an + x_j)\sin(\gamma \mp \varepsilon_c) \mp (bv + y_j)\sin\varepsilon_c. \end{cases} \tag{32}$$

The range of the v index is governed by the second chirality index of the layer: $v = 0, \ldots, (p_m - 1)$. The atomic coordinates with the chiral indexes [equation (15)] can be deduced from equation (32):

$$\begin{cases} \rho_{mnvj} = \{\rho_{0m}^2 + \frac{1}{2\pi^2}[(an + x_j)(pb\cos\gamma \pm sa) \\ \qquad +(bv + y_j)(pb \pm sa\cos\gamma)]\}^{1/2} + z_j \\ \varphi_{mnvj} = \frac{1}{\tau}\left(\{\rho_{0m}^2 + \frac{1}{2\pi^2}[(an + x_j)(pb\cos\gamma \pm sa) \right. \\ \qquad \left. +(bv + y_j)(pb \pm sa\cos\gamma)]\}^{1/2} - \rho_m\right) \\ z_{mnvj} = z_{0m} + \frac{\sin\gamma}{2\pi d}[pb(an + x_j) \mp sa(bv + y_j)]. \end{cases} \tag{33}$$

3.4. Azimuthally monoclinic scroll nanotube

The deviation of the chiral angle or inner radius from the conditions (16) and (28) will lead to structural changes of the initial orthogonal nanotube. In such cases an ordered scroll nanotube of longitudinally monoclinic (if the chiral angle changes) or azimuthally monoclinic (if the inner radius changes) polytypic modification is formed. This section describes the structure of an azimuthally monoclinic scroll nanotube and conditions of its formation.

From equation (20) it follows that a change of the inner radius $\Delta\rho_0$ causes a change of the length along the flat spiral from its initial point to the starting point of the mth turn:

$$\xi'_m = 2\pi(\rho_0 + \Delta\rho_0)m + \pi m^2 d = \xi_m + 2\pi\Delta\rho_0 m, \tag{34}$$

where ρ_0 is the inner radius of the unchanged spiral or orthogonal scroll tube. Fig. 10 represents the planar layer of the lattice that is similar to Fig. 7. Heavy red lines represent the unchanged turn borders, while black lines show changed ones. Heavy arrows represent chiral vectors $\mathbf{r}'^{m}_{sp}$ of the changed

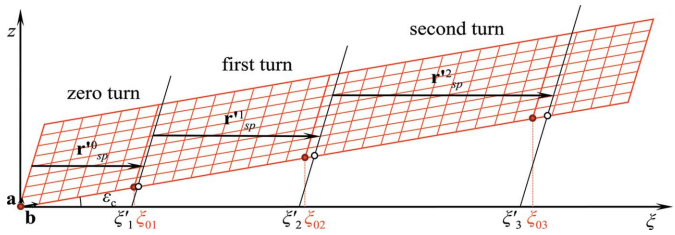

Figure 10
The development of an azimuthally monoclinic lattice that belongs to a right-handed scroll nanotube.

lattice. According to expressions (22) and (24) the lengths of the changed turns are

$$\begin{aligned} L'_m &= \xi'_{m+1} - \xi'_m = \xi_{m+1} + 2\pi\Delta\rho_0(m+1) - \xi_m - 2\pi\Delta\rho_0 m \\ &= L_m + 2\pi\Delta\rho_0. \end{aligned}$$

In accordance with equation (23), the differences between the adjacent turns are

$$\begin{aligned} \Delta L'_m &= L'_{m+1} - L'_m = L_{m+1} + 2\pi\Delta\rho_0 - L_m - 2\pi\Delta\rho_0 \\ &= \Delta L_m = 2\pi d, \end{aligned}$$

(*i.e.* have the same value). The achieved result and equation (30) allow us to present the magnitude of the chiral vector of the mth turn in a similar way to equation (26):

$$\begin{aligned} r'^{m}_{sp} &= L'_0 + 2\pi dm = L_0 + 2\pi\Delta\rho_0 + 2\pi dm \\ &= 2\pi\rho_0 + \pi d + 2\pi dm + 2\pi\Delta\rho_0. \end{aligned}$$

The chiral vector with the unchanged generator (s, p) can also be presented in a similar way to equation (9). It should be noticed that in this case the chiral vector is not a vector of the plane lattice.

For a semi-multiple initial orthogonal lattice, it is easy to achieve expressions analogous to equation (28) by using the chiral vectors' parallelism property:

$$\begin{aligned} s'_0 &= s\frac{\rho'_0 + d/2}{d} = s\frac{\rho_0 + d/2}{d} + s\frac{\Delta\rho_0}{d} = s(m_0 + t), \\ p'_0 &= p\frac{\rho'_0 + d/2}{d} = p(m_0 + t), \end{aligned}$$

where $\rho'_0 = \rho_0 + \Delta\rho_0$, and parameter $t = \Delta\rho_0/d$ has ranges $0 < t < 1$. If $t = 0$ ($\Delta\rho_0 = 0$) or $t = 1$ ($\Delta\rho_0 = d$) we will get an orthogonal tube, which is equivalent to the initial one. Consequently, the chiral indexes (s'_m, p'_m) of the azimuthally monoclinic nanotube turns are

$$s'_m = s(m_0 + m + t), \quad p'_m = p(m_0 + m + t).$$

Because of the smallness of the t parameter, the v index, which determines the nodes in the direction parallel to **b**, has unchanged ranges: $v = 0, \ldots, [p(m_0 + m) - 1]$. In the general case, the inner radius of the azimuthally monoclinic scroll nanotube is not a multiple of the layer thickness or its half, and the chiral indexes (s'_m, p'_m) of the turns are not integers.

Determination of the atomic coordinates of an azimuthally monoclinic scroll nanotube requires coordinates of the initial nodes ($n = 0$, $v = 0$; marked by red points in Fig. 10) belonging

to lattice turns. From Fig. 10 it is clearly seen that, in the present case, in contrast to an orthogonal tube, the initial node of each turn (apart from zero turn) is shifted relative to the border of the turn. The positions of these nodes are governed by the integer number of b parameters [equation (31)] in the direction parallel to **b** (Fig. 10). Consequently, the atomic coordinates of the initial nodes of the mth turn (Fig. 10) are

$$z_{0m} = \mp P_m b \sin\varepsilon_c,$$
$$\xi_{0m} = P_m b \cos\varepsilon_c \rightarrow \rho_{0m} = [(\rho_0 + \Delta\rho_0)^2 + 2\tau\xi_{0m}]^{1/2}, \quad (35)$$

where equation (19) is also used. By using the achieved results and equations (1), (19) and (21), it is possible to determine the cylindrical atomic coordinates of the mth turn:

$$\begin{cases} \rho_{mnvj} = \{\rho_{0m}^2 + 2\tau[(an + x_j)\cos(\gamma \mp \varepsilon_c) \\ \qquad +(bv + y_j)\cos\varepsilon_c]\}^{1/2} + z_j \\ \varphi_{mnvj} = \frac{1}{\tau}(\{\rho_{0m}^2 + 2\tau[(an + x_j)\cos(\gamma \mp \varepsilon_c) \\ \qquad +(bv + y_j)\cos\varepsilon_c]\}^{1/2} - \rho'_m) \\ z_{mnvj} = z_{0m} + (an + x_j)\sin(\gamma \mp \varepsilon_c) \mp (bv + y_j)\sin\varepsilon_c, \end{cases}$$

where $\rho'_m = \rho'_0 + md = \rho_0 + \Delta\rho_0 + md$ is the changed initial radii of the flat spiral turns. After expansion of the trigonometric functions in terms of the chiral indexes using equation (15), we will get

$$\begin{cases} \rho_{mnvj} = \{\rho_{0m}^2 + \frac{1}{2\pi^2}[(an + x_j)(pb\cos\gamma \pm sa) \\ \qquad +(bv + y_j)(pb \pm sa\cos\gamma)]\}^{1/2} + z_j \\ \varphi_{mnvj} = \frac{1}{\tau}(\{\rho_{0m}^2 + \frac{1}{2\pi^2}[(an + x_j)(pb\cos\gamma \pm sa) \\ \qquad +(bv + y_j)(pb \pm sa\cos\gamma)]\}^{1/2} - \rho'_m) \\ z_{mnvj} = z_{0m} + \frac{\sin\gamma}{2\pi d}[pb(an + x_j) \mp sa(bv + y_j)]. \end{cases}$$

The difference between z coordinates of the initial nodes belonging to adjacent turns can be deduced from equation (35) after taking into account (16):

$$z_{0,m+1} - z_{0m} = \mp(P_{m+1} - P_m)b\sin\varepsilon_c = \mp pb(m_0 + m)\sin\varepsilon_c$$
$$= \mp s(m_0 + m)a\sin(\gamma \mp \varepsilon_c). \quad (36)$$

The value $a\sin(\gamma \mp \varepsilon_c)$ is equal to the projection of the a parameter on the axis of the tube and, therefore, the difference [equation (36)] corresponds to the relative shift of the adjacent layers to the integer numbers of a in the **a** direction. Consequently, the character of the relative positions of the turns in the longitudinal direction is equivalent to the orthogonal lattice. Relative positions of the turns in the circumferential direction can be deduced from the difference between the initial nodes' ξ coordinate (ξ_{0m}) determined by equation (35), and the mth turn starting point ξ coordinate that is governed by

$$\xi'_{0m} = P'_m b\cos\varepsilon_c, \quad P'_m = \sum_{m=0}^{m-1} p'_m = p\left(m_0 + t + \frac{m-1}{2}\right)m.$$

When

$$\xi'_{0m} - \xi_{0m} = P'_m b\cos\varepsilon_c - P_m b\cos\varepsilon_c = bp\frac{\Delta\rho_0}{d}m\cos\varepsilon_c,$$

that is similar to the azimuthally monoclinic polytype of the ordered coaxial lattice. Here the value $pb(\Delta\rho_0/d)\cos\varepsilon_c$ has the same meaning as the $\Delta\xi$ parameter in coaxial tubes. Figs. 11(a) and 11(b) represent the comparative pictures of the orthogonal and azimuthally monoclinic polytypic modifications of the scroll achiral nanotube.

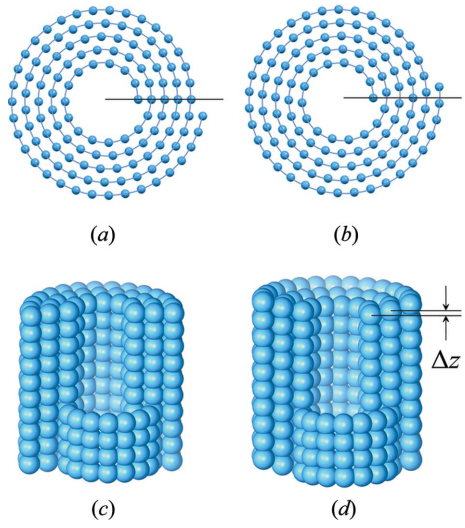

Figure 11
Achiral scroll lattices. (a) Orthogonal ($m_0 = 3$), top view. (b) Azimuthally monoclinic ($m_0 = 3$, $\Delta\xi = b/3$), top view. (c) Orthogonal ($m_0 = 2$, $\Delta\varepsilon = 0°$), side view. (d) Longitudinally monoclinic (chiral, $m_0 = 2$, $\Delta\varepsilon = 1°$), side view.

3.5. Longitudinally monoclinic scroll nanotube

Let us examine the shift of scroll nanotube turns at a change of chiral angle. For this purpose, we will consider the longitudinally monoclinic scroll nanotube, which is based on the orthogonal tube from §3.3. The chiral angle ε_c and initial radius of the orthogonal tube ρ_0 correspond to the generator with integer parameters (s, p). If deviation $\Delta\varepsilon$ of the chiral angle occurs, then the changed chiral angle is equal to $\varepsilon'_c = \varepsilon_c + \Delta\varepsilon$. Such a procedure corresponds to rotation of a primary orthogonal lattice on the surface of the scroll relative to the initial point of its lattice. The magnitudes of chiral vectors are governed by the same [equation (30)] expression because parameters of the scroll surface do not change, although in this case chiral vectors of the scroll are not lattice vectors because the layer is rotated on the angle $\Delta\varepsilon$. Fig. 12 shows develop-

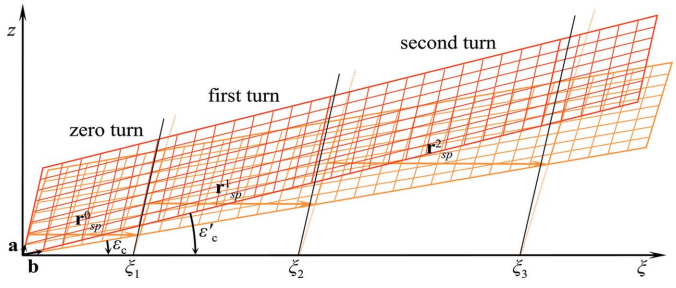

Figure 12
The developments of longitudinally monoclinic and orthogonal lattices of a right-handed scroll nanotube.

ments of layers that correspond to orthogonal (yellow lines) and longitudinally monoclinic (red lines) right-handed scroll lattices. The layer of monoclinic lattices is rotated on the angle $\Delta\varepsilon$ relative to the orthogonal one. The borders of the turns are represented on the same figure by dashed lines (orthogonal polytype) and solid lines (longitudinally monoclinic polytype) converging at ξ_m points; the chiral vectors of the orthogonal lattice are represented by arrows. Here transformation (1) has the form

$$\begin{cases} \xi'_{nvj} = (an + x_j)\cos(\gamma \mp \varepsilon'_c) + (bv + y_j)\cos\varepsilon'_c \\ z'_{nvj} = (an + x_j)\sin(\gamma \mp \varepsilon'_c) \mp (bv + y_j)\sin\varepsilon'_c. \end{cases} \quad (37)$$

Let us deduce the chiral indexes of the turn that belongs to a longitudinal monoclinic scroll lattice. Fig. 13(*a*) shows the lattice of the turn with initial node ($n = 0, v = 0$) represented by the red point. Chiral triangles governed by the vector equalities $\mathbf{r}^m_{sp} = -s_m\mathbf{a} + p_m\mathbf{b}$ and $\mathbf{r}'^m_{sp} = -s'_m\mathbf{a} + p'_m\mathbf{b}$, which correspond to the mth turn of orthogonal (yellow lines) and longitudinally monoclinic (black lines) lattices, are also represented in Fig. 13(*a*). In our analysis we consider that all nodes corresponding to the turn of the initial orthogonal lattice belong to the turn of the longitudinally monoclinic lattice after rotation. Chirality indexes (s'_m, p'_m) of the mth turn that corresponds to the longitudinally monoclinic lattice can be expressed as

$$s'_m = s_m + \Delta s_m, \quad p'_m = p_m + \Delta p_m,$$

where (s_m, p_m) are chiral indexes of the orthogonal lattice's mth turn. From the equality of the chiral vector magnitudes

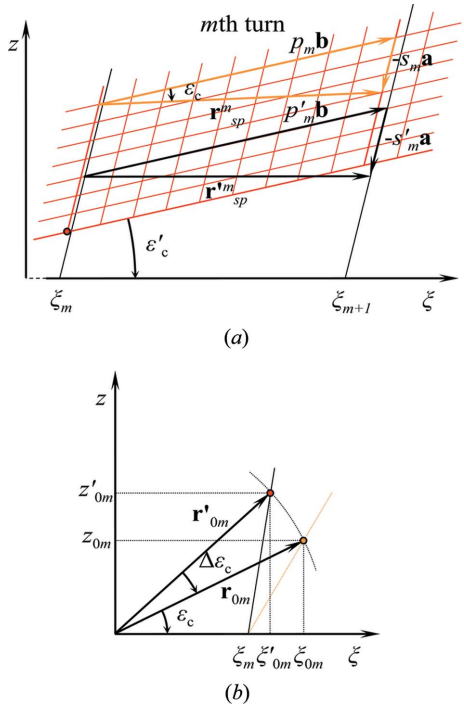

Figure 13
(*a*) The relative positions of the mth turn's developments of orthogonal and longitudinally monoclinic scroll nanotubes. (*b*) The determination of the first node position of the longitudinally monoclinic nanotube's turn.

and the sine law applied to chiral triangles ($\mathbf{r}^m_{sp} = \pm s_m\mathbf{a} + p_m\mathbf{b}$ and $\mathbf{r}'^m_{sp} = \pm s'_m\mathbf{a} + p'_m\mathbf{b}$), we get

$$\frac{s_m a}{\sin\varepsilon_c} = \frac{r^m_{sp}}{\sin\gamma} = \frac{p_m b}{\sin(\gamma \mp \varepsilon_c)},$$
$$\frac{s'_m a}{\sin\varepsilon'_c} = \frac{r^m_{sp}}{\sin\gamma} = \frac{p'_m b}{\sin(\gamma \mp \varepsilon'_c)}.$$

Therefore,

$$\frac{s_m a}{\sin\varepsilon_c} = \frac{s'_m a}{\sin\varepsilon'_c} \rightarrow \Delta s_m = s_m\left(\frac{\sin\varepsilon'_c}{\sin\varepsilon_c} - 1\right), \quad s'_m = s_m\frac{\sin\varepsilon'_c}{\sin\varepsilon_c},$$

and

$$\frac{p_m b}{\sin(\gamma \mp \varepsilon_c)} = \frac{p'_m b}{\sin(\gamma \mp \varepsilon'_c)} \rightarrow \Delta p_m = p_m\left[\frac{\sin(\gamma \mp \varepsilon'_c)}{\sin(\gamma \mp \varepsilon_c)} - 1\right],$$
$$p'_m = p_m\frac{\sin(\gamma \mp \varepsilon'_c)}{\sin(\gamma \mp \varepsilon_c)}.$$

The transfer of the planar layer onto the mth turn of the longitudinally monoclinic scroll nanotube requires, as in previous cases, the coordinates of initial nodes ($n = 0$, $v = 0$) belonging to lattice turns. Fig. 13(*b*) shows initial nodes of the orthogonal (yellow point) and longitudinally monoclinic (red point) scroll lattices having (ξ_{0m}, z_{0m}) and (ξ'_{0m}, z'_{0m}) coordinates. From §3.3 it follows that the magnitudes of corresponding lattice vectors are

$$r'_{0m} = r_{0m} = \frac{\xi_{0m}}{\cos\varepsilon_c} = P_m b.$$

Consequently, from Fig. 13(*b*) and equation (19) it follows that

$$z'_{0m} = \mp P_m b\sin\varepsilon'_c,\ \xi'_{0m} = P_m b\cos\varepsilon'_c,\ \rho'_{0m} = (\rho_0^2 + 2\tau\xi'_{0m})^{1/2}.$$

Cylindrical coordinates of the atoms of a longitudinally monoclinic scroll nanotube could be deduced from equations (19), (21) and (37):

$$\begin{cases} \rho_{mnvj} = \{\rho'^2_{0m} + 2\tau[(an + x_j)\cos(\gamma \mp \varepsilon'_c) \\ \qquad +(bv + y_j)\cos\varepsilon'_c]\}^{1/2} + z_j \\ \varphi_{mnvj} = \frac{1}{\tau}\left(\{\rho'^2_{0m} + 2\tau[(an + x_j)\cos(\gamma \mp \varepsilon'_c) \right. \\ \qquad \left. +(bv + y_j)\cos\varepsilon'_c]\}^{1/2} - \rho_m\right) \\ z_{mnvj} = z'_{0m} + (an + x_j)\sin(\gamma \mp \varepsilon'_c) \mp (bv + y_j)\sin\varepsilon'_c. \end{cases}$$

It is easy to express trigonometric functions in terms of chiral indexes by using expression (15):

$$\begin{aligned}
\sin\varepsilon'_{\rm c} &= \sin(\varepsilon_{\rm c}+\Delta\varepsilon) = \sin\varepsilon_{\rm c}\cos\Delta\varepsilon + \cos\varepsilon_{\rm c}\sin\Delta\varepsilon \\
&= \frac{sa\sin\gamma}{2\pi d}\cos\Delta\varepsilon + \frac{pb \pm sa\cos\gamma}{2\pi d}\sin\Delta\varepsilon \\
&= \frac{\Delta^{s1}_{sp}}{2\pi d}, \\
\sin(\gamma \mp \varepsilon'_{\rm c}) &= \sin(\gamma \mp \varepsilon_{\rm c} \mp \Delta\varepsilon) \\
&= \sin(\gamma \mp \varepsilon_{\rm c})\cos\Delta\varepsilon \mp \cos(\gamma \mp \varepsilon_{\rm c})\sin\Delta\varepsilon \\
&= \frac{pb\sin\gamma}{2\pi d}\cos\Delta\varepsilon \mp \frac{pb\cos\gamma \pm sa}{2\pi d}\sin\Delta\varepsilon \\
&= \frac{\Delta^{s2}_{sp}}{2\pi d}, \\
\cos\varepsilon'_{\rm c} &= \cos(\varepsilon_{\rm c}+\Delta\varepsilon) = \cos\varepsilon_{\rm c}\cos\Delta\varepsilon - \sin\varepsilon_{\rm c}\sin\Delta\varepsilon \\
&= \frac{pb \pm sa\cos\gamma}{2\pi d}\cos\Delta\varepsilon - \frac{sa\sin\gamma}{2\pi d}\sin\Delta\varepsilon \\
&= \frac{\Delta^{c1}_{sp}}{2\pi d}, \\
\cos(\gamma \mp \varepsilon'_{\rm c}) &= \cos(\gamma \mp \varepsilon_{\rm c} \mp \Delta\varepsilon) \\
&= \cos(\gamma \mp \varepsilon_{\rm c})\cos\Delta\varepsilon \pm \sin(\gamma \mp \varepsilon_{\rm c})\sin\Delta\varepsilon \\
&= \frac{pb\cos\gamma \pm sa}{2\pi d}\cos\Delta\varepsilon \pm \frac{pb\sin\gamma}{2\pi d}\sin\Delta\varepsilon \\
&= \frac{\Delta^{c2}_{sp}}{2\pi d},
\end{aligned}$$

where $\Delta^{s1}_{sp} = pb\sin\Delta\varepsilon + sa\sin(\gamma \pm \Delta\varepsilon)$, $\Delta^{s2}_{sp} = pb\sin(\gamma \mp \Delta\varepsilon) - sa\sin\Delta\varepsilon$, $\Delta^{c1}_{sp} = pb\cos\Delta\varepsilon \pm sa\cos(\gamma \pm \Delta\varepsilon)$, $\Delta^{c2}_{sp} = pb\cos(\gamma \mp \Delta\varepsilon) \pm sa\cos\Delta\varepsilon$. Atomic coordinates with chiral indexes can be expressed in the form:

$$\begin{cases}
\rho_{mnvj} = \left\{\rho'^2_{0m} + \frac{1}{2\pi^2}[(an+x_j)\Delta^{c2}_{sp} + (bv+y_j)\Delta^{c1}_{sp}]\right\}^{1/2} + z_j \\
\varphi_{mnvj} = \frac{1}{\tau}\left(\{\rho'^2_{0m} + \frac{1}{2\pi^2}[(an+x_j)\Delta^{c2}_{sp} \right. \\
\qquad \left. +(bv+y_j)\Delta^{c1}_{sp}]\}^{1/2} - \rho_m\right) \\
z_{mnvj} = z'_{0m} + \frac{1}{2\pi d}[(an+x_j)\Delta^{s2}_{sp} \mp (bv+y_j)\Delta^{s1}_{sp}],
\end{cases}$$

where

$$\begin{aligned}
z'_{0m} &= \mp\frac{P_m b}{2\pi d}\Delta^{s1}_{sp}, \quad \xi'_{0m} = \frac{P_m b}{2\pi d}\Delta^{c1}_{sp}, \\
\rho'_{0m} &= \left(\rho_0^2 + 2\tau\frac{P_m b}{2\pi d}\Delta^{c1}_{sp}\right)^{1/2}. \qquad (38)
\end{aligned}$$

Expression (38) allows us to deduce a relative position of turns. In the longitudinal direction the shift could be expressed as

$$z'_{0,m+1} - z'_{0m} = \mp(P_{m+1} - P_m)\frac{b\Delta^{s1}_{sp}}{2\pi d} = \mp\frac{pb\Delta^{s1}_{sp}}{2\pi d}(m_0 + m).$$

It means that, in general, the relative shift of the adjacent layers is not equal to the integer number of a, as it was in the azimuthally monoclinic polytype. In the circumferential direction the relative shift is

$$\xi'_{0,m+1} - \xi'_{0m} = (P_{m+1} - P_m)\frac{b\Delta^{c1}_{sp}}{2\pi d} = \frac{pb\Delta^{c1}_{sp}}{2\pi d}(m_0 + m).$$

The deduced relative shift is similar to the azimuthally monoclinic case. Consequently, the interlayer shift has a monoclinic character in both directions in the longitudinally monoclinic scroll nanotube. In the case of a small chiral angle, the angular displacement will produce a quite considerable longitudinal shift, while a circumferential shift will be near zero (Figs. 11*c* and 11*d*). Substantial similarity of the interlayer shifts presented in Figs. 5(*c*), 5(*d*) and Figs. 11(*c*), 11(*d*) should also be noted.

4. Conclusions

Studies of ordered nanotube structure and conditions of their formation have led to different conclusions with regard to coaxial and cylindrical scroll lattices.

It is known from several works (Hamada *et al.*, 1992; Zhang *et al.*, 1993; Bernaerts *et al.*, 1998; Saito *et al.*, 1998; Amelinckx *et al.*, 1999; Qin, 2006; Nasyrov *et al.*, 2010) that chiral indexes having integer values promote continuity of a cylindrical lattice on each layer. The existence of the lattice vector (generator of the cylindrical lattice) with a magnitude that is equal to the circumference of the 'unit' circle governs the possibility of close-packed structure formation. Close-packed nanotubes are monochiral and have chiral vectors that are a multiple of the generator. In the presented work it was shown that the radii of the layers belonging to the close-packed coaxial nanotube are a multiple of the layer thickness. The deviation from monochirality or multipleness of the layers should be treated as a defect. The interlayer shift, that governs the polytypic modifications, might have an ordered or random character.

Cylindrical scroll nanotubes are close packed and monochiral by definition. The inner radius and chiral angle unambiguously define the structure of a nanotube and exclude the possibility of interlayer parameters being random. Deviations of a chiral angle (defined by the generator) or an inner radius from the multiple or semi-multiple values lead to the creation of the longitudinal or azimuthal polytypic modifications of scroll nanotubes. Therefore, in contrast to coaxial tubes, such deviation could not be treated as a structure defect. According to our research, any scroll lattice is ordered, while the existence of an integer generator governs only the possibility of orthogonal polytype formation.

The formation of an ordered coaxial nanotube requires an integral generator and, therefore, such a condition can be used as a criterion for the study of layered compounds, which can (geometrically) form these tubular structures. Scroll structures do not have the restrictions mentioned above.

APPENDIX *A*
List of the main parameters used in this article

a, lattice basis vector of the nanotube layer that has a direction closest to its axis.
b, lattice basis vector of the nanotube layer that has a direction closest to its cross-sectional plane.
γ, angle between lattice basis vectors **a** and **b**.
d, thickness of the nanotube layer.

Δa, parameter that defines a shift of one layer relative to another along the vector **a**.
Δb, parameter that defines a shift of one layer relative to another along the vector **b**.
n, index number of the nodal turn (or nodal circle) of the nanotube layer: $n = 0; 1; 2; 3; \ldots N - 1$, N, number of lattice rows along the nanotube axis.
m, index number of the nanotube layer: $m = 0; 1; 2; 3 \ldots M - 1$, M, number of layers in the nanotube.
m_0, multiplicity factor of the inner radius: $m_0 = 0; 1; 2; 3 \ldots$.
v, index number of the node on the nodal turn (or nodal circle) of the nanotube: $v = 0; 1; 2; 3; \ldots p_m - 1$.
j, index number of the atom in the unit cell.
x_j, coordinate of the jth atom in the unit cell determined along **a**.
y_j, coordinate of the jth atom in the unit cell determined along **b**.
z_j, coordinate of the jth atom in the unit cell determined along the normal to the nanotube surface (out-of-plane).
ρ_m, radii of the mth layer of the nanotube or radii of the beginning point of its mth turn.
ρ_{mj}, the distance of the jth atom in the unit cell on the mth layer from the nanotube axis.
ρ_0, inner radius of the nanotube.
φ_{mnvj}, azimuthal coordinate of the jth atom in the vth unit cell on the nth turn (or nodal circle) standing on the mth layer of the nanotube (cylindrical coordinate of the jth atom in the circumferential direction).
Φ, azimuthal variable of the Archimedean spiral, φ is the same variable within a single turn.
$\{\rho, \varphi, z\}$, cylindrical system in which the z axis coincides with the nanotube axis.
$\{a, b\}$, oblique coordinate system.
$\{\xi, z\}$, rectangular coordinate system.
ε_m, circumferential shift of the mth layer relative to the common reference point.
ε_c, chiral angle of the nanotube.
s_m, the number of lattice nodes that determine the pitch of the screw along nodal row with v = const on the mth layer of the nanotube (chiral index of the nanotube's mth layer).
p_m, the number of lattice nodes on the turn (or circle) on the mth layer of the nanotube (the second chiral index); P_m, the total number of lattice nodes on the m turns.
s'_m, first chiral index of the monoclinic scroll nanotube's mth layer.
p'_m, second chiral index of the monoclinic scroll nanotube's mth layer.
ε'_c, chiral angle of the longitudinally monoclinic scroll nanotube; $\Delta\varepsilon$, its deviation from the orthogonal case; Δs_m and Δp_m, corresponding deviations of the chiral indexes.
$\Delta\rho_0$, deviation of the inner radius of the azimuthally monoclinic scroll nanotube from the orthogonal case.
Δz, longitudinal shift of the monoclinic nanotube.
Δz_m, longitudinal shift of the mth coaxial layer relative to the common reference point.
$\Delta\xi$, circumferential shift of the monoclinic nanotube.
ξ_m, length along the spiral to the beginning of the mth turn.
ξ'_m, length along the spiral to the beginning of the mth turn of azimuthally monoclinic scroll nanotubes.
$\mathbf{r}_{sp}$, generator of the cylindrical lattice, where s and p are its components.
$\mathbf{r}_j$, vector that defines the position of the atom in the projection of the unit cell on a plane.
$\mathbf{r}_{nv}$, the vector of the plane lattice.
$\mathbf{r}_{nvj}$, the vector that defines the position of the atom in the structure of the planar layer.
$\mathbf{r}^m_{sp}$, the chiral vector of the nanotube's mth layer.
L_m, the length of the circumference of the circle (plane spiral turn) that corresponds to the mth layer (mth turn) in the cross-sectional plane of the nanotube.
L'_m, the length of the plane spiral that corresponds to the mth turn in the cross-sectional plane of the azimuthally monoclinic scroll nanotube.

Acknowledgements

We acknowledge the Cambridge Crystallographic Data Centre (CCDC) for the *Mercury* program provided at no cost that we used in visualization of crystal structures.

References

Amelinckx, S., Devouard, B. & Baronnet, A. (1996). *Acta Cryst.* A**52**, 850–878.
Amelinckx, S., Lucas, A. & Lambin, P. (1999). *Rep. Prog. Phys.* **62**, 1471–1524.
Aruja, E. (1943). PhD thesis, University of Cambridge, England.
Bandura, A. V. & Evarestov, R. A. (2009). *Surf. Sci.* **603**, L117–L120.
Baronnet, A., Mellini, M. & Devouard, B. (1994). *Phys. Chem. Miner.* **21**, 330–343.
Bates, T. F., Sand, L. B. & Mink, J. F. (1950). *Science*, **111**, 512–513.
Bernaerts, D., Amelinckx, S., Lambin, P. & Lucas, A. A. (1998). *Appl. Phys. A Mater. Sci. Process.* **67**, 53–64.
Bernaerts, D., De Beeck, M. O., Van Landijyt, S. A. J. & Tendeloo, G. (1996). *Philos. Mag. A*, **74**, 723–740.
Cheng, G., Calizo, I., Liang, X., Sperling, B. A., Johnston-Peck, A. C., Li, W., Maslar, J. E., Richter, C. A. & Hight Walker, A. R. (2014). *Carbon N. Y.* **76**, 257–265.
DeVouard, B. & Baronnet, A. (1995). *Eur. J. Mineral.* **7**, 835–846.
Enyashin, A. N. & Seifert, G. (2005). *Phys. Status Solidi (b)*, **242**, 1361–1370.
Hamada, N., Sawada, S. & Oshiyama, A. (1992). *Phys. Rev. Lett.* **68**, 1579–1581.
Hong, S. Y., Popovitz-Biro, R., Prior, Y. & Tenne, R. (2003). *J. Am. Chem. Soc.* **125**, 10470–10474.
Iijima, S. (1991). *Nature (London)*, **354**, 56–58.
Jagodzinski, H. & Kunze, G. (1954). *Neues Jahrb. Miner. Monatsh.* **7**, 137–150.
Khalitov, Z., Khadiev, A. & Pashin, D. (2015). *J. Appl. Cryst.* **48**, 29–36.
Nasyrov, I. K., Pashin, D. M., Khalitov, Z. Y. & Valeeva, D. N. (2010). *Sci. Isr. Technol. Advantages*, **12**, 63–73.
Noll, W. & Kircher, H. (1951). *Neues Jahrb. Miner.* **10**, 219–240.
Noll, W. & Kircher, H. (1952). *Naturwissenschaften*, **39**, 233–234.
Padurow, N. N. (1950). *Acta Cryst.* **3**, 204–208.
Pauling, L. (1930). *Proc. Natl Acad. Sci. USA*, **16**, 578–582.
Qin, L.-C. (2006). *Rep. Prog. Phys.* **69**, 2761–2821.
Radovsky, G., Popovitz-Biro, R., Staiger, M., Gartsman, K., Thomsen, C., Lorenz, T., Seifert, G. & Tenne, R. (2011). *Angew. Chem. Int. Ed.* **50**, 12316–12320.

Saito, R., Dresselhaus, G. & Dresselhaus, M. S. (1998). *Physical Properties of Carbon Nanotubes*. London: Imperial College Press.
Warren, B. E. & Bragg, W. L. (1931). *Z. Kristallogr. Cryst. Mater.* **76**, 201–210.
Whittaker, E. J. W. (1951). *Acta Cryst.* **4**, 187–188.
Whittaker, E. J. W. (1952). *Acta Cryst.* **5**, 143–144.
Whittaker, E. J. W. (1953). *Acta Cryst.* **6**, 747–748.
Whittaker, E. J. W. (1954). *Acta Cryst.* **7**, 827–832.
Whittaker, E. J. W. (1955*a*). *Acta Cryst.* **8**, 571–574.
Whittaker, E. J. W. (1955*b*). *Acta Cryst.* **8**, 265–271.
Xie, X., Ju, L., Feng, X., Sun, Y., Zhou, R., Liu, K., Fan, S., Li, Q. & Jiang, K. (2009). *Nano Lett.* **9**, 2565–2570.
Yada, K. (1967). *Acta Cryst.* **23**, 704–707.
Yada, K. (1971). *Acta Cryst.* A**27**, 659–664.
Yada, K. & Iishi, K. (1977). *Am. Mineral.* **62**, 958–965.
Zhang, X. F., Zhang, X. B., Van Tendeloo, G., Amelinckx, S., Op de Beeck, M. & Van Landuyt, J. (1993). *J. Cryst. Growth*, **130**, 368–382.
Zhao, J., Yang, B., Yang, Z., Zhang, P., Zheng, Z., Ren, W. & Yan, X. (2014). *Carbon N. Y.* **79**, 470–477.